Journal of Materials Science: Materials in Electronics
https://doi.org/10.1007/s10854-019-02484-6

Effect of Mn^{2+} as a redox additive on ternary doped polyaniline-metal nanocomposite: an efficient dielectric material

C. Anju[1] · Shiny Palatty[2]

Received: 24 August 2019 / Accepted: 30 October 2019

Abstract
An efficient ternary doped polyaniline-metal nanocomposite was synthesized via in situ rapid mixing chemical oxidative polymerization method. The detailed morphological and structural analysis shows the incorporation of binary transition metals (Fe & Mn) in a highly crystalline PANI matrix with a modified flaky morphology. Further dielectric and electrochemical characterizations substantiate a high dielectric constant and specific capacitance of about 613F/g with a good cyclic stability for the as synthesized PANI material.

1 Introduction

With the continuous growth of global economy, the demand for high performing energy storage and conversion devices like supercapacitors [1–7], Li based batteries [8–12], solar cell [13] etc. are on its high due to energy crisis and global warming issues. Conducting polymers (polyaniline, polypyrrole, polyacetylene, poly (3,4-ethylenedioxythiophene), transition metal oxides ($FeO_2{\cdot}H_2O$, $MnO_2{\cdot}H_2O$, Fe_2O_3, MnO_2, NiO) and hydroxides ($Ni(OH)_2$ and $Co(OH)_2$) are still the pseudocapacitive material of interest of the investigators [14–16] due to the combined contributions from faradaic reactions and electrochemical adsorption/desorption of ions at the electrode/electrolyte interface thereby acquiring a higher capacitance compared to that of EDLC's [17]. Much effort has been devoted by the researchers for the development of multicomponent hybrid material with specific properties by the appropriate introduction of inorganic phases in the polymer matrix which is a key factor in all the energy devices. Also high dielectric constant polymer nanocomposites are an integral part of capacitor technology since they have been continuously explored by the electronic industries to meet the energy requirement [18].

The large pseudocapacitance originated from the redox reactions of pi conjugated backbone made conducting polymer, a widely investigated energy storing material, where the charge can be stored in whole volume [19, 20]. Among these conducting polymer, PANI, a P-type semiconductor known as aniline black has the longest history due to its low cost, ease of synthesis, acid doping, base-dedoping chemistry, excellent environmental stability and good conductivity [21]. The versatility of PANI lies on the fact that its physical and electrochemical properties can be tailored to specific application since it can be moulded in various shapes and dimensions through chemical oxidative polymerization by altering its synthetic conditions [22]. The high pseudocapacitance benefited from various oxidation states due to the presence of interconvertible quinoid and benzenoid rings by electron transfer, porous nature and high surface area makes PANI an ideal supercapacitive material [23, 24]. But the poor cycle stability of PANI is the major hindrance of its applicability in energy devices which can be surpassed by developing composite designs with transition metals. The presence of active amine group in polyaniline chain makes it an ideal substrate for the introduction of transition metal or metal oxide nano particle due to the unique electron exchange property where the resultant PANI nanocomposites possess unique properties like good dielectric responses and stability which are inherited from its individual components [25, 26].

Electronic supplementary material The online version of this article (https://doi.org/10.1007/s10854-019-02484-6) contains supplementary material, which is available to authorized users.

✉ Shiny Palatty
shinypalaty@gmail.com

C. Anju
anju.chonat@gmail.com

[1] Department of Basic Sciences & Humanities, Rajagiri School of Engineering & Technology, Ernakulam, Kerala 682039, India

[2] Department of Chemistry, Bharata Mata College, Ernakulam, Kerala 682021, India

Published online: 11 November 2019

Transition metals, with its multiple coordination ability can form interchain linkages with the amine and imine nitrogen sites of PANI [27]. Also the presence of metal nano particles in the PANI matrix can provide short diffusion path length and high electroactive region thereby facilitating the easier access of electrolyte into the electrode surface which helps to achieve superior electrochemical activity suitable for energy storage and conversion applications [20, 28]. These transition metals can also perform as a redox-active catalyst thereby enhancing the energy density and capacitance of the final PANI composite [29].

The doping is a redox reaction which causes an increment or decrement in the electronic number by transforming a neutral molecule into an ionic macromolecule where the charge neutralization will be done by the counter ion [23]. Many researchers are now interested on the synthesis of PANI containing multiple dopants especially transition metal dopants where the modified physical and chemical properties of the polymer composite depends on the character of metal used. Also morphology is a critical factor upon which the capacitive performance of PANI based material depends where the type of dopant used plays a significant role in modifying the structure [30].

Although PANI and its composites have been widely synthesized by different methods, the investigation on the electrochemical performance is still an extensive area of research. It is essential that electronic conduction, capacitance and stability of PANI should be enhanced so as to use it as a supercapacitive material which can be achieved via transition metals. Thus the objective of the present article is to synthesize a ternary doped polyaniline-metal nanocomposite through rapid mixing chemical oxidative polymerization method by utilizing ferric chloride as oxidant (which itself can take the role of a dopant) and $MnSO_4$ & HCl as external binary dopants and to investigate its dielectric properties and electrochemical performances through Cyclic voltammetry (CV) and Electrochemical Impedance Spectroscopy (EIS) analysis. Further morphological, structural and electronic properties of the resultant composite are studied through SEM, TEM, FT-IR, XRD & UV–Vis characterisations.

2 Experimental methods and materials

2.1 Materials

Aniline ($C_6H_5NH_2$) was double distilled prior to use. Anhydrous Ferric chloride ($FeCl_3$), Manganous sulphate monohydrate ($MnSO_4{\cdot}H_2O$), Hydrochloric acid (HCl) and acetone (CH_3COCH_3) were of analytical grade and were used without any treatment. All the above materials were supplied by Merck (India). Throughout the preparation procedures deionized water was used.

2.2 Synthesis of ternary doped polyaniline-metal nanocomposite

Ternary doped PANI was synthesized via in situ chemical oxidative rapid mixing polymerization method using $FeCl_3$ as oxidant (also act as a dopant) in 1 M HCl medium. In order to prepare PANI nanocomposites, different concentrations of $MnSO_4$ (0.3, 0.5, 0.7 & 1 M) prepared in deionized water was added to 0.1 M aniline solution and the resultant aniline-manganese solution was stirred at a constant speed for half an hour using a magnetic stirrer. After that the oxidant 0.3 M $FeCl_3$ made in 1 M HCl dopant (initially stirred for 10–15 min) was rapidly added to the above prepared aniline-manganese solution. Without any agitation the solution was kept overnight and the resultant dark green precipitate of PANI was filtered using vacuum pump. The washing process was done by using deionized water and acetone until the filtrate become colourless. Finally it was dried in an air oven for 24 h at 80 °C. For comparison PANI was also prepared by using 1 M HCl dopant by the same procedure as above.

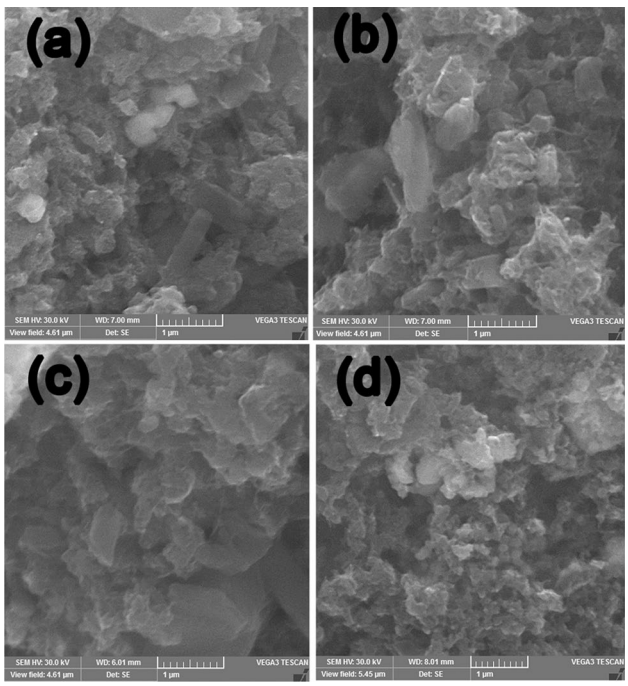

Fig. 1 SEM image of ternary doped PANI with **a** (0.3 M Mn^{2+} + 1 M HCl) **b** (0.5 M Mn^{2+} + 1 M HCl) **c** (0.7 M Mn^{2+} + 1 M HCl) **d** (1 M Mn^{2+} + 1 M HCl)

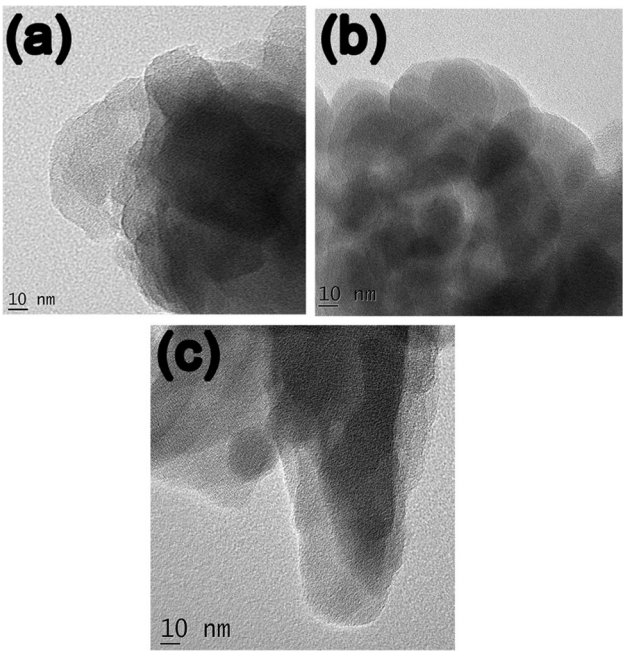

Fig. 2 TEM image of ternary doped **a** (0.7 M Mn^{2+} + 1 M HCl) **b** (1 M Mn^{2+} + 1 M HCl) **c** binary doped PANI (1 M HCl)

2.3 Morphological, structural, dielectric and electrochemical characterization

In order to characterize the surface morphology of ternary doped PANI Scanning electron microscopy (SEM) was used. The sample is smeared on a small piece of adhesive carbon tape which is fixed on a brass stub. The sample, then subjected to gold coating using sputtering unit (model: JFC1600) for 10 s at 10 mA of current. The gold coated sample placed in chamber of SEM (Jeol, JSM 6390LA) and secondary electron/Back Scattered electron images are recorded. Also the types of transition metals coordinated with the PANI nitrogen is confirmed by SEM–EDS analysis where elemental analysis carried out in the scanned area/point/line using EDAX detector. The coating of PANI surface with transition metal cations was further observed by using High resolution-Transmission electron spectroscopy (HR-TEM) (Jeol/JEM 2100 with LaB_6 source with resolution Point: 0.23 nm, Lattice: 0.14 nm). An extremely small amount of material is suspended in ethanol. The solution is homogenized using ultrasonicator to disperse the particles. A drop of the solution is then pipetted out and cast the drop on carbon-coated grids of 200 mesh the grid is dried and fixed in the specimen holder.

The chemical structure, crystallinity and composition of PANI were studied by using (1) Fourier transform infrared spectroscopy (FT-IR) (Thermo Nicolet, Avatar 370 at a frequency range 4000–400 cm^{-1} and a resolution of 4 cm^{-1}). The sample was added to KBr and pelletized and the pellet was analysed to obtain the spectra (2) UV–Vis spectroscopy (Varian, Cary 5000 in a spectral range of 175–3300 nm with a wavelength accuracy of about ± 0.1 nm). The spectra are taken between 200 and 800 nm. The finely powdered sample is filled in the solid state sample holder and analysis is carried out (3) X-ray diffraction (XRD) (Bruker AXS D8 Advance with CuKa radiation operating at a wavelength of 1.5406 Å) with current and operating voltage at 40 mA and 40 kV. The XRD analysis was carried out in the 2theta ranges from 10° to 75°. The frequency depend dielectric parameters like dielectric constant, tangent loss and ac conductivity measurements was done by using Agilent LCR meter on compressed PANI pellets (Agilent LCR series meter—E4980 A) in a frequency range from 100 Hz to 2 MHz. The electrochemical characterizations were evaluated by using

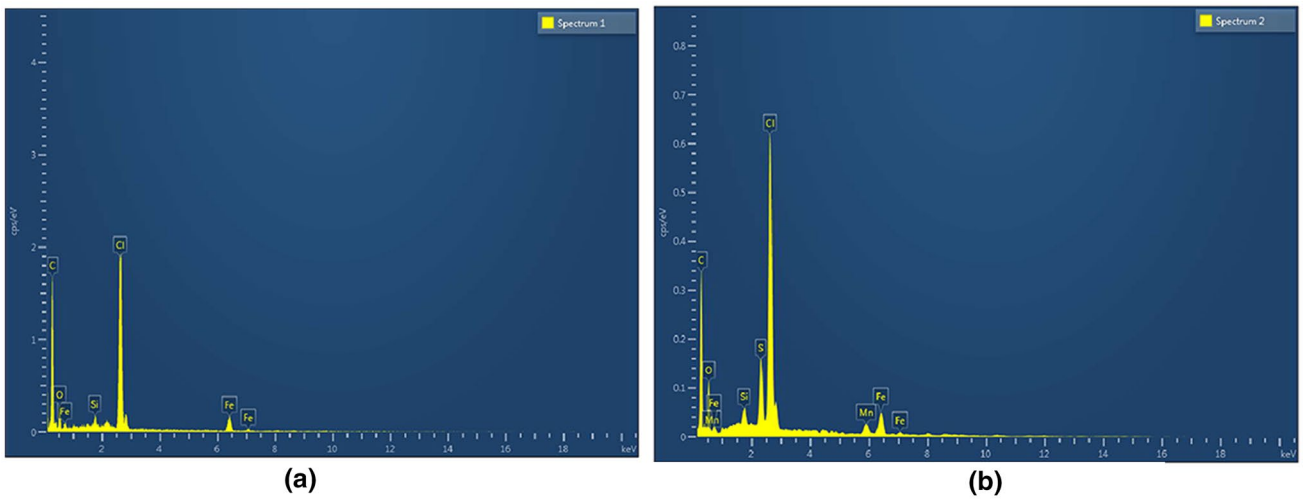

Fig. 3 SEM–EDS analysis of **a** binary doped PANI with 1 M HCl **b** ternary doped PANI with (0.7 M Mn^{2+} + 1 M HCl)

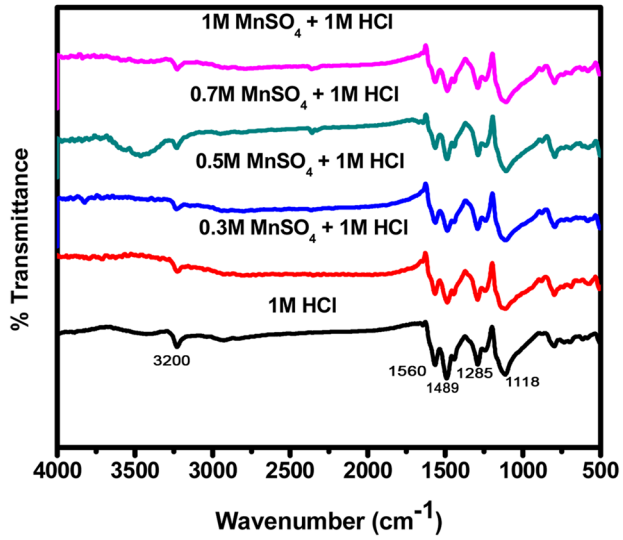

Fig. 4 FT-IR spectra of ternary doped PANI at different concentrations and Binary doped PANI with 1 M HCl

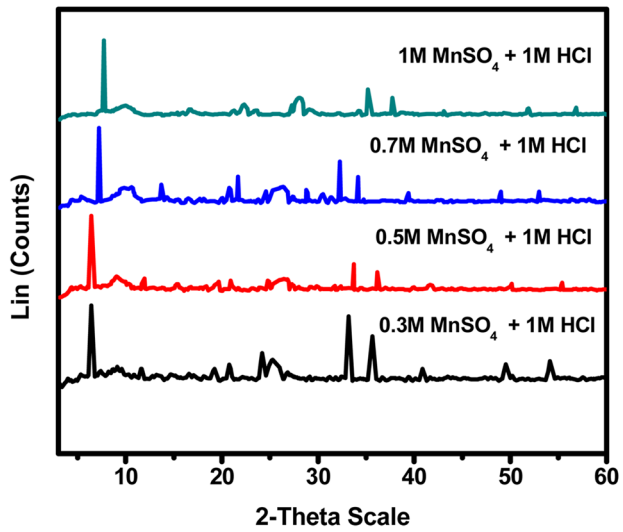

Fig. 5 XRD pattern of ternary doped PANI at different concentrations

cyclic voltammetry (CV) (EG&G potentiostat (model 263A) which is interfaced to a PC through a GPIBcard (National instruments)) and Electrochemical Impedance spectroscopy analysis (EIS) (5210 lock-in amplifier Perkin-Elmer instruments) with Powersuite software (EG&G) interfaced with a PC) and the testing was done in 0.1 M H_2SO_4 electrolyte using a three electrode system (working electrode–graphite electrode), counter electrode-Platinum foil and a reference electrode (Ag/AgCl/3 M NaCl). CV was studied in a potential window from − 0.1 to 0.6 V at different scan rates 10, 20, 50, 100 and 200 mV/s and EIS testing was measured in a frequency range from 100 MHz to 100 kHz.

Dielectric constant, tangent loss and ac conductivity were calculated using the equations $\varepsilon' = C\ d/\varepsilon^0 A$, $\tan\delta = \epsilon''/\epsilon'$ and $\sigma ac = 2\Pi f \epsilon'' \varepsilon^0$, respectively, where C is the capacitance measured, d—thickness, A—area of the pellet, ε^0 is the dielectric permittivity in vacuum (8.85×10^{-12} Fm^{-1}), ϵ'—dielectric constant, ϵ''—dielectric loss and f—applied frequency (Hz).

The mass specific capacitance value was calculated using the equation

$$C_{sp} = \frac{\int_{v_1}^{v_2} i(v)dv}{(v_2 - v_1)ms}$$

where numerator represents the total charge under CV curve, $(v_2 - v_1)$ is the potential window, mis the mass of the electrode and s is the scan rate.

3 Results and discussions

3.1 Morphological characterization

Morphological study i.e. the chain alignment of PANI is very crucial for the exploitation of PANI properties for desired applications. The surface morphology of as prepared PANI sample was studied by electron microscopy (SEM & TEM) analysis and it reveals the strong influence of dopants ratio in tuning PANIs surface. The ternary doped PANI composite has the advantageous characteristics due to the presence of binary transition metals Fe and Mn which can form interchain linkages by coordinating nitrogen atoms at different sites on PANI chain [29]. Such bridging can result in flaky or plate like structure as seen in the SEM image of ternary doped PANI (Fig. 1a–c). TEM micrographs (Fig. 2c) (SI-1) confirmed branched fibre like morphology for HCl doped PANI but a clear morphological modification i.e. a flake like surface is observed when Mn^{2+} was used as a dopant. The presence of phenazine segments (supported by FT-IR) can act as an additional substrate for the growth of PANI in flake form. At higher concentration of Mn^{2+}(1 M) more agglomeration is seen (Fig. 1d) and the corresponding TEM image (Fig. 2b) confirmed the formation of spherical morphology due to more inter and intra chain linkage formations.

The attachment of various transition metals (Fe and Mn) with the PANI nitrogen is further confirmed by SEM–EDS analysis (Fig. 3) (SI-2). The analysis results illustrate the successful incorporation of both Fe and Mn in PANI matrix where the reacting tendency of both the metals shows a clear difference. The coordination tendency of Fe (from the oxidant) is more than manganese which can be further substantiated by the stable electronic configuration of Mn^{2+} than

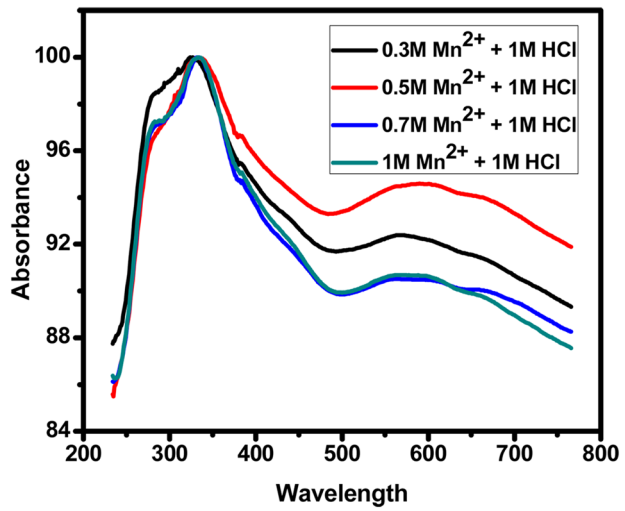

Fig. 6 UV–Vis spectra of ternary doped PANI at different concentrations

Fe^{3+}. Thus the above results confirmed the role of binary transition metals (Fe & Mn) to obtain good surface morphological features and properties for PANI.

3.2 Structural characterization

The FT-IR analysis of ternary and binary doped PANI samples was depicted in the Fig. 4 (SI-3). The appearance of characteristics peaks around 1560 and 1489 cm^{-1} denotes C=C stretching vibrations of quinoid and benzenoid units and those at 1285 and 1225 cm^{-1} indicates C–N stretching in quinoid and benzenoid moieties. The N–H stretching vibration is indicated by the peak around 3200 cm^{-1}. The formation of emeraldine salt form of PANI is reflected by the peak around 1118 cm^{-1} and the band at lower wave numbers around 784 cm^{-1} is an indication of C–H bending vibrations [31–33]. Also the Peak around 1429 cm^{-1} denotes ring stretching of phenazine unit formed by intramolecular cyclization between PANI chains and branched oligoaniline [34]. The ternary doped PANI has its peaks around 1548, 1485, 1273, 1224 and 1106 cm^{-1}. The above spectral features reveals that the ternary doped PANI spectrum has very much resemblance with HCl doped PANI. But when compared to HCl doped PANI FT-IR peaks of ternary doped PANI samples shows some blue shift due to the change in electron density near quinoid and benzenoid moieties where C–N bond is perturbed due to the coordination of nitrogen with binary transition metals Fe and Mn [34]. The blue shift also confirms the enhancement in the doping level and improved delocalization due to the electron withdrawing effect of Mn [35]. Most of the peaks of the ternary doped PANI are broader than binary doped (1 M HCl doped) PANI which justifies the additional incorporation of transition metal Mn other than Fe (from the oxidant) with PANI matrix. The intensity ratio of the bands I_{1560}/I_{1489} which reflects the extent of oxidation [36] in HCl doped and ternary doped are almost similar suggesting the interaction of ternary dopants with PANI does not much alter its transport properties like conjugation length, doping level etc. [37].

3.3 XRD

Unlike a conventional polymer system, pi–pi interactions in relatively stiff charged polyconjugated chain can provide fairly good ordered domains in PANI matrix [38]. But the extent of crystallinity strongly relies on the type of dopant, oxidant, reaction conditions and the morphology. The detailed structural analysis of PANI nano composite was

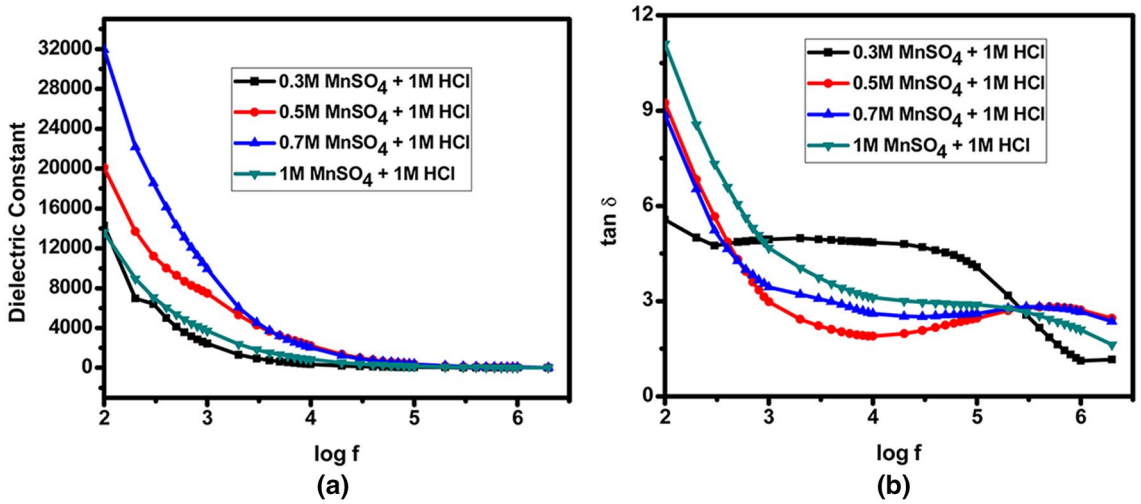

Fig. 7 Frequency dependence of **a** dielectric constant **b** tangent loss of ternary doped PANI at different concentrations

done by using XRD technique. The X-ray diffractogram (Fig. 5) (SI-4) shows the crystal characteristics of PANI synthesized by using ternary dopants with $MnSO_4$ at different concentrations from 0.3 M to 1 M and ferric chloride oxidant. The diffractogram points that ternary doped PANI are highly crystalline and the diffraction peaks located at 2theta values 14, 20 and 25 represents (011), (020) and (200) planes of emeraldine salt form of PANI [39]. The peaks at 20 and 25 indicate periodicity parallel and perpendicular to PANI chains. The appearance of crystalline peaks in lower 2theta values (around 6.5 and 12) further confirmed highly ordering in PANI chains. Khalid et al. claimed that the periodic distance between the dopant and the N atom on adjacent chains results in a peak around 6.5 [40]. Also additional peaks are noticed at higher 2 theta values (around 33, 35, 40, 50, 54) pointing towards the formation of metal nano particles. At 0.3 M Mn^{2+}, the intensity of the peaks at higher 2 theta values are high compared to 0.7 M Mn^{2+} indicating the formation of more number of metal oxides in PANI matrix. But with the increase in concentration of Mn^{2+} from 0.3 to 0.7 M, XRD pattern shows the formation of highly crystalline PANI and the existence of metal oxide nanoparticles in smaller nano sizes, suggesting the formation of good conducting PANI samples and thereafter a decline in crystallinity is observed at higher concentration (1 M Mn^{2+}). These results confirmed that polymer doping state has strong impact in deciding the extent of crystalline characteristics [34]. Thus the XRD pattern concluded that although the crystallinity is very much preserved in all the above prepared PANI samples, 0.7 M Mn^{2+} with 1 M HCl combination has the highest crystallinity which is in good agreement with the conductivity measurements. The highest crystallinity acquired at 0.7 M Mn^{2+} concentration is associated with the formation of more flake like structures where such plate like moieties can promote high ordering of PANI chains. All the above data strongly substantiates the influence of ternary dopants ratio in tuning PANIs chemical structure. Thus the synergistic effect of binary transition metals Fe, Mn and the inorganic dopant HCl modifies the crystalline phase of PANI and thereby its transport properties [41] (supported by ac conductivity studies) which are the essentials to perform as an supercapacitive material.

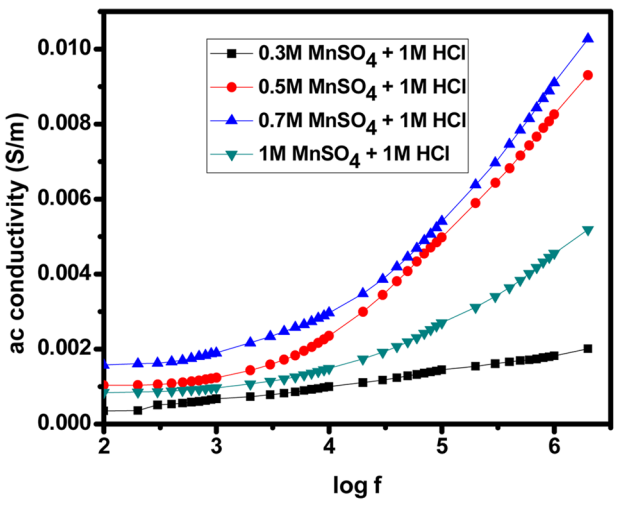

Fig. 8 Frequency dependence of ac conductivity of ternary doped PANI at different concentrations

3.4 UV–Visible

To check the influence of binary transition metal cations on the electronic properties of ternary doped PANI, UV–Vis spectroscopy analysis was done. UV–Vis spectra (Fig. 6) indicate the as synthesized ternary doped PANI in its emeraldine salt form with its distinctive peak formations around 330 nm, shoulder peak around 390 nm and a long tail in the near-IR region around 600 nm which is the characteristics of polaron bands [42]. The absorption around 330 nm is ascribed to π–π* transitions of the benzenoid ring of PANI. The localized polaron-π* and π to polaron transition results in peaks around 380 and 600 nm, respectively. With the increase in doping level of manganese a decrement in the intensity of absorption peak at higher wavelength is observed which explains the interaction of more number of dopant cations to form a coiled morphology (supported by morphological analysis) [42] due to multiple interaction with PANIs nitrogen at different sites. PANIs imine and amine nitrogen interaction with the metal cations might substantially withdraw the intensity of orbital overlap between phenyl rings pi electrons and nitrogen lone pairs [43]. Also the formation of more number of phenazine segments at higher concentration could reduce the intensity of π to polaron transition [44].

3.5 Frequency dependent dielectric and AC conductivity studies

The applicability of as synthesized PANI material in energy storage application was first assessed through dielectric studies in a frequency range 100 Hz to 2 MHz at room temperature. Figure 7a, b displays the frequency dependent dielectric constant and tangent loss values of PANI synthesized using different concentrations of Mn^{2+}. The dielectric constant and tangent loss values are related to the stored and lost energy under an external field and they show a similar behaviour i.e. at lower frequency side the values are high due to Maxwell–Wagner–Sillars (MWS) interfacial polarization effect [6, 45] and thereafter it decreases and forms a plateau at high frequency side due to dielectric relaxation phenomenon indicating that the external frequency variations easily affects the charge carrier localization [46]. Both

the dielectric constant and tangent loss have constant values in a log frequency range above 5.

With the increase in concentration of Mn^{2+} dielectric constant value reached a maximum of 31955 at 0.7 M Mn^{2+} concentration and thereafter the value starts declining at higher Mn loading to 13602. With the increase in the concentration of Mn^{2+} more charge carriers accumulate in internal interfaces, thus increasing interfacial polarization and dielectric constant values [47]. The improvement in dielectric constant value is attributed to the coordination of binary transition metals (Fe & Mn) with imine and amine nitrogen which can cause more charge delocalization and the flaky morphology helps to carry more charges due to the advantage of high surface to volume ratio. Also the Mn loading induces more regularity (supported by xrd) in PANI matrix which further improves charge traps and space-charge densities [45]. At higher concentration (1 M Mn^{2+}) due to the attachment of more number of metal cations, PANI chain gets agglomerated which can block the conductive path way and reduces interfacial polarization. Thus the optimal Mn concentration was chosen as 0.7 M for electrochemical performances.

The calculated tangent loss values for different PANI samples are 5.6 (0.3 M Mn), 9.2 (0.5 M Mn), 8.9 (0.7 M Mn) and 11 (1 M Mn) at low frequency side and all of them shows a lower loss values at high frequency side. The decreased tangent loss values at high frequency side could be due to the inability of weakly bound electrons for long range migration and might be due to "the skin effect" phenomenon which increases the resistivity of the samples [48]. As the concentration of Mn^{2+} increases, loss values increases due to more leakage current [45] except at 0.7 M Mn^{2+} and the decreased loss value at this concentration might be attributed to its highly crystalline modified surface morphology which effectively carries more charges. Thus it can be concluded that the addition of stoichiometric proportion of Mn^{2+} to the PANI matrix could substantially decrease the leakage current and finally the loss values.

3.6 AC conductivity

Due to the complex structural and morphological forms the electrical properties of PANI, a p-type semiconductor involves a large number of charge transport mechanisms [49]. The frequency dependent transport property of PANI is shown in the Fig. 8. From the graph it is clear that ac conductivity is a frequency dependent parameter where at low frequency region the value remains almost constant and at high frequency side above the critical frequency the ac conductivity raises exponentially obeying the power law [25]. The improved conductivity at high frequency portion is attributed to the movement of polarons and bipolarons along the polymer chain.

The heterogeneous semi crystalline PANI system is related to a quasi metallic island surrounded by non-metallic amorphous zone [50]. The electrical conductivity of PANI is due to the inter and intra chain hopping mechanism into the crystalline area. In the crystalline area the hopping mechanism of polarons are responsible for electrical conduction while in the amorphous region intergrain resonance tunnelling occurs through the strongly localized states [36]. From the graph it is shown that with the increase in concentration of Mn from 0.3 to 0.7 M ac conductivity increases from 0.0004 to 0.002 S/m. The improved doping levels can create new energy levels in between valence band and the conduction band by the overlap of polarons and bipolarons which decreases the band gap thereby facilitating the electron jump to the conduction band. The highest conductivity acquired at 0.7 M Mn^{2+} concentration is highly connected with the flaky morphology which can rise high ordering of PANI chains and finally the conductivity [51]. At higher concentration of Mn (1 M) entangling of PANI chains blocks the conductive pathway thereby decreases the conductivity.

3.7 Electrochemical characterization

The electrochemical characterisation of ternary doped PANI material was studied by using Cyclic voltammetry and Electrochemical Impedance analysis in 0.1 M H_2SO_4 electrolyte using a three electrode system. CV was performed in a potential window from −0.1 to 0.6 V at different scan rate 10, 20, 50, 100 and 200 mV/s.

3.7.1 Cyclic voltammetry

The CV of ternary doped PANI (0.7 M Mn^{2+} + 1 M HCl) displays the characteristics rectangular shape which is the peculiarity of electrical double layer capacitor. The typical oxidation and reduction peaks observed in the CV curve are the contributions from faradaic reactions which is associated with leucoemeraldine/emeraldine and emeraldine/pernigraniline transitions [52]. These kinds of redox reactions are responsible for the pseudocapacitive behaviour of PANI. Also the shift to various oxidation sates may affect the conductivity and finally the redox reactions of PANI [53]. The presence of transition metal cations (Fe & Mn) in ternary doped PANI has a significant role in overcoming such defects due to its inherent coordination tendency with the PANI nitrogen which can enhance the capacitance value [29]. Further this kind of coordination can ensures good ionic diffusion by enhancing the conductive channels and by decreasing the diffusion length [54].

The CV curve of ternary doped PANI at different scan rates are shown in the Fig. 9b. Due to the electrode resistance a shift in the oxidation and reduction peaks are observed with the increase in scan rate. The calculated specific

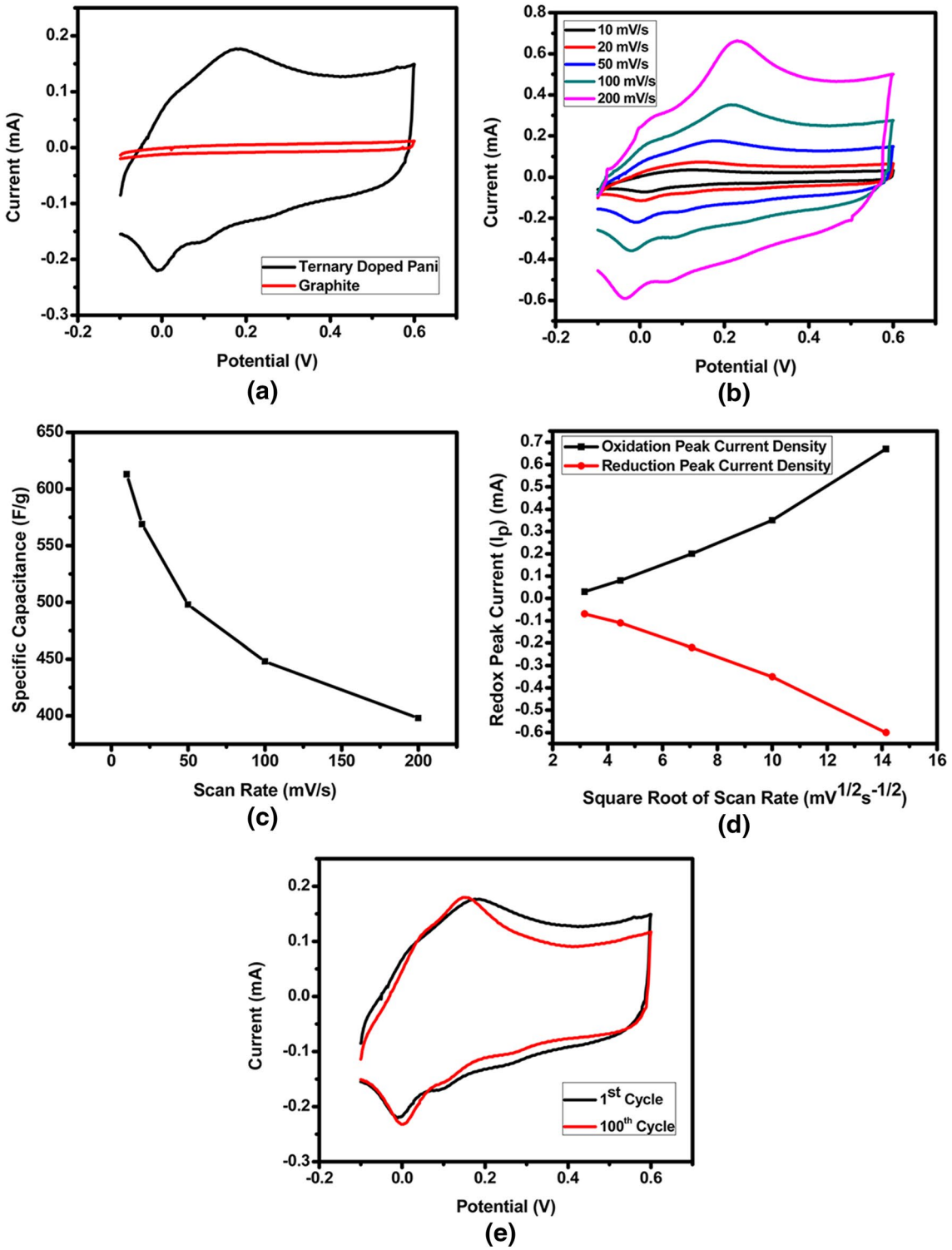

Fig. 9 **a** CV voltammogram of (0.7 M Mn^{2+} + 1 M HCl) ternary doped PANI and bare graphite at a scan rate 50 mV/s **b** CV voltammogram of (0.7 M Mn^{2+} + 1 M HCl) ternary doped PANI at different scan rate **c** Specific capacitance of (0.7 M Mn^{2+} + 1 M HCl) ternary doped PANI at different scan rate **d** Plot of oxidation and reduction peak current versus square root of scan rate of (0.7 M Mn^{2+} + 1 M HCl) ternary doped PANI **e** CV voltammogram of (0.7 M Mn^{2+} + 1 M HCl) ternary doped PANI at a scan rate of 50 mV/s after 100 cycles

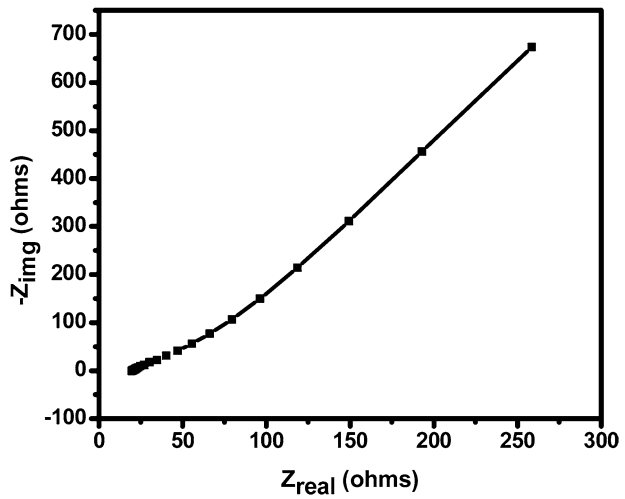

Fig. 10 Nyquist plot of (0.7 M Mn^{2+} + 1 M HCl) ternary doped PANI in a frequency range from 100 MHz to 100 kHz

capacitance values are 613, 569, 498, 448 and 398F/g at 10, 20, 50, 100 & 200 mV/s, respectively. The degradation in the specific capacitance value from 613 to 398F/g (Fig. 9c) can be assigned to the diffusion effect of proton within the electrodes and the enhanced specific capacitance value observed at lower scan rate is attributed to the formation of inner active sites which can undergo redox reactions [29]. The linear correlation between redox peak current and square root of scan rate (Fig. 9d) was an indication of a surface-confined redox process [55]. Good rate ability of ternary doped PANI is substantiated by the improved peak current (shown by the enhancement in the magnitude of cathodic and anodic peak) with the increase in scan rate with the retention of CV curve pattern where the increased peak current at higher scan rate is related to faster ionic transport [56].

In order to further confirm the capacitive response of ternary doped PANI cycling performance (Fig. 9e) was evaluated after 100 cycles at a scan rate of 50 mV/s which is a significant indicator for real life applications. Even after the long run not much degradation in the capacitance is observed pointing to descent structural stability of PANI. The transition metal cations can act as an electron acceptor site to stabilize PANI. Also the metal cations could easily bridge the adjacent PANI chains due to multiple coordination ability thereby overcome the most lethal deficiency of instability issue of PANI during rapid charge–discharge process [27]. Thus the synergistic effect of ternary dopants meliorates the electrochemical stability of PANI.

3.7.2 Electrochemical impedance spectroscopy (EIS)

In order to fortify the enhanced electrochemical performance of ternary doped PANI, EIS is an informative technique to evaluate the electrical, structural and charge transport properties at electrode–electrolyte interface [29]. The frequency response of electrode–electrolyte interaction was analysed using electrochemical impedance spectroscopy by plotting Nyquist plot and is depicted in the Fig. 10. The low frequency region in the typical nyquist plot carries a vertical line and an inconspicuous arc in the high frequency portion. The formation of semi circle formation is attributed to the resistor like behaviour of a ideal capacitor [57] which is related with interface effects and the vertical line is an indication of faradaic pseudocapacitance. The overall resistance and capacitance behaviour of the PANI can be predicted from the nature of nyquist plot [57]. The above nyquist plot has a very small semi circle portion with a smaller diameter indicating a minimal internal resistance which might be attributed to ternary doping process and an efficient binding of PANI chains with Fe and Mn and the straight line is more vertical suggesting a closest approach to an ideal capacitor i.e. a better pseudocapacitive performance [58]. The resistance is inversely proportional to transfer rate of ions i.e. the minimal resistance indicates a faster charge transport [59]. Thus the ability of as designed ternary doped PANI material for energy storage applications can be concluded by the following reasons (1) enhanced coordination of binary transition metal cations (Fe & Mn) with nitrogen atom of PANI which facilitates charge transport (2) high crystallinity (3) Decreased electrochemical degradation due to the improved adhesion strength of PANI through multiple coordination (4) modified flake like morphology which can effectively carries the charges and improved the contact space between PANI and electrolytic solution (5) Good ionic diffusion due to enhanced conductive channels and shortened diffusion length

4 Conclusion

An efficient pseudocapacitive material, ternary doped polyaniline-metal nanocomposite was successfully synthesized via in situ rapid mixing polymerization method by the stoichiometric combination of two pseudocapacitive materials- PANI and the transition metals Fe & Mn. The presence of binary transition metals enhances the electroactive sites and the polyaniline acts as a conductive pathway. The as synthesized ternary doped PANI composite is highly crystalline with excellent dielectric and electrochemical properties and has a specific capacitance of about 613F/g. We also demonstrate that the modified flaky surface morphology obtained in ternary doped PANI-metal nano composite (0.7 M Mn^{2+} + 1 M HCl) has a positive influence on the pseudocapacitive behaviour due to high surface to volume ratio.

Acknowledgements The authors acknowledge Director and Principal, Rajagiri School of Engineering & Technology and Bharata Mata College for the support of this work. Analytical support from Sophisticated Test and Instrumentation Centre, CUSAT, School of Pure & Applied Physics, Mahatma Gandhi University and Department of Physics, Maharajas College are also acknowledged.

Compliance with ethical standards

Conflict of interest There are no conflicts to declare.

References

1. K. Le, M. Gao, W. Liu, J. Liu, Z. Wang, F. Wang, V. Murugadoss, S. Wu, T. Ding, Z. Guo, MOF-derived hierarchical core-shell hollow iron-cobalt sulfides nanoarrays on Ni foam with enhanced electrochemical properties for high energy density asymmetric supercapacitors. Electrochim. Acta **323**, 134826 (2019). https://doi.org/10.1016/j.electacta.2019.134826
2. W. Du, X. Wang, J. Zhan, X. Sun, L. Kang, F. Jiang, X. Zhang, Q. Shao, M. Dong, H. Liu, V. Murugadoss, Z. Guo, Biological cell template synthesis of nitrogen-doped porous hollow carbon spheres/MnO_2 composites for high-performance asymmetric supercapacitors. Electrochim. Acta (2018). https://doi.org/10.1016/j.electacta.2018.11.074
3. K. Le, Z. Wang, F. Wang, Q. Wang, Q. Shao, V. Murugadas, S. Wu, W. Liu, J. Liu, Q. Gao, Z. Guo, Sandwich-like NiCo layered double hydroxides/reduced graphene oxide nanocomposite cathode for high energy density asymmetric supercapacitors. Dalton Trans. (2019). https://doi.org/10.1039/c9dt00615j
4. Y. Ma, M. Ma, X. Yin, Q. Shao, N. Lu, Y. Feng, Y. Lu, Tuning polyaniline nanostructures via end group substitutions and their morphology dependent electrochemical performances. Polymer (2018). https://doi.org/10.1016/j.polymer.2018.09.051
5. Y. Ma, C. Hou, H. Zhang, Q. Zhang, H. Liu, S. Wu, Electrochimica acta three-dimensional core-shell Fe_3O_4/Polyaniline coaxial heterogeneous nanonets: preparation and high performance supercapacitor electrodes. Electrochim. Acta **315**, 114–123 (2019). https://doi.org/10.1016/j.electacta.2019.05.073
6. K. Sun, J. Dong, Z. Wang, Z. Wang, G. Fan, Q. Hou, L. An, M. Dong, R. Fan, Z. Guo, Tunable negative permittivity in flexible graphene/PDMS metacomposites. J. Phys. Chem. C (2019). https://doi.org/10.1021/acs.jpcc.9b06753
7. Y. Zhang, Y. An, L. Wu, H. Chen, Z. Li, H. Dou, V. Murugadoss, J. Fan, X. Zhang, X. Mai, Z. Guo, Metal-free energy storage systems: combining batteries with capacitors based on methylene blue functionalized graphene cathode. Mater. Chem. A (2019). https://doi.org/10.1039/C9TA06734E
8. Y. Zhai, J. Wang, Q. Gao, Y. Fan, C. Hou, Y. Hou, H. Liu, Q. Shao, S. Wu, L. Zhao, T. Ding, F. Dang, Z. Guo, Highly efficient cobalt nanoparticles anchored porous N-doped carbon nanosheets electrocatalysts for Li-O_2 batteries. J. Catal. **377**, 534–542 (2019). https://doi.org/10.1016/j.jcat.2019.07.055
9. C. Hou, J. Wang, W. Du, J. Wang, Y. Du, C. Liu, J. Zhang, H. Hou, F. Dang, L. Zhao, Z. Guo, Molybdenum carbide heterostructures coupled with 3D holey carbon nanosheets for highly efficient and ultrastable cycling lithium-ion. J. Mater. Chem. A **7**, 13460–13472 (2019). https://doi.org/10.1039/c9ta03551f
10. M. Liu, Z. Yang, H. Sun, C. Lai, X. Zhao, H. Peng, T. Liu, A hybrid carbon aerogel with both aligned and interconnected pores as interlayer for high-performance lithium—sulfur batteries. Nano Res. (2016). https://doi.org/10.1007/s12274-016-1244-1
11. M. Liu, Y. Liu, Y. Yan, F. Wang, J. Liu, T. Liu, A highly conductive carbon-sulfur film with interconnected mesopores as advanced cathode for lithium-sulfur batteries. ChemComm (2017). https://doi.org/10.1039/C7CC04523A
12. J. Tian, Q. Shao, X. Dong, J. Zheng, D. Pan, X. Zhang, H. Cao, L. Hao, J. Liu, X. Mai, Z. Guo, Electrochim. Acta (2018). https://doi.org/10.1016/j.electacta.2017.12.094
13. V. Murugadas, J. Lin, H. Liu, X. Mai, T. Dina, Z. Guo, S. Angaiah, Optimizing graphene content in nise/graphene nanohybrid counter electrode on boosting photovoltaic performance of dye-sensitized solar cells. Nanoscale (2019). https://doi.org/10.1039/C9NR07060E
14. Y. Xie, X. Sha, Electrochemical cycling stability of nickel (II) coordinated polyaniline. Synth. Met. **237**, 29–39 (2018). https://doi.org/10.1016/j.synthmet.2018.01.011
15. C. Hu, S. Chen, Y. Wang, X. Peng, W. Zhang, J. Chen, Excellent electrochemical performances of cabbage-like polyaniline fabricated by template synthesis. J. Power Sources **321**, 94–101 (2016). https://doi.org/10.1016/j.jpowsour.2016.04.113
16. H. Guan, L. Fan, H. Zhang, X. Qu, Polyaniline nanofibers obtained by interfacial polymerization for high-rate supercapacitors. Electrochim. Acta **56**, 964–968 (2010). https://doi.org/10.1016/j.electacta.2010.09.078
17. Y. Wang, Y. Song, Y. Xia, Characterization and applications chemical functional materials. Chem. Soc. Rev. **45**, 5925–5950 (2016). https://doi.org/10.1039/C5CS00580A
18. M.N. Nadagouda, R.S. Varma, Green approach to bulk and template-free synthesis of thermally stable reduced polyaniline nanofibers for capacitor applications. Green Chem. **9**, 632 (2007). https://doi.org/10.1039/b614633c
19. S.A. El-khodary, G.M. El-enany, M. El-okr, M. Ibrahim, Modified iron doped polyaniline/sulfonated carbon nanotubes for all symmetric solid-state supercapacitor. Synth. Met. **233**, 41–51 (2017). https://doi.org/10.1016/j.synthmet.2017.09.002
20. S. Ghosh, T. Maiyalagan, R.N. Basu, Nanostructured conducting polymers for energy applications: towards a sustainable platform. Nanoscale **8**, 6921–6947 (2016). https://doi.org/10.1039/C5NR08803H
21. G. Ciri, Recent advances in polyaniline research: polymerization mechanisms, structural aspects, properties and applications. Synth. Met. **177**, 1–47 (2013). https://doi.org/10.1016/j.synthmet.2013.06.004
22. D.M. Jundale, S.T. Navale, G.D. Khuspe, D.S. Dalavi, P.S. Patil, V.B. Patil, Polyaniline-CuO hybrid nanocomposites: synthesis, structural, morphological, optical and electrical transport studies. J. Mater. Sci.: Mater. Electron. (2016). https://doi.org/10.1007/s10854-013-1280-5
23. E. Hur, A. Arslan, Cobalt ion-doped polyaniline, poly(-methylaniline), and poly(-ethylaniline): electrosynthesis and characterisation using electrochemical methods in acidic solutions. Chem. Papers (2014). https://doi.org/10.2478/s11696-014-0605-z
24. L. Tang, F. Duan, M. Chen, Fabrication of ferric chloride doped polyaniline/multilayer super-short carbon nanotube nanocomposites for supercapacitor applications. J. Solid State Electrochem. (2016). https://doi.org/10.1007/s10008-016-3264-x
25. L.N. Shubha, P. Madhusudana Rao, Temperature characterization of dielectric permittivity and AC conductivity of nano copper oxide-doped polyaniline composite. J. Adv. Dielectr. **6**, 1650018 (2016). https://doi.org/10.1142/s2010135x16500181
26. C. Li, H. Bai, G. Shi, Conducting polymer nanomaterials: electrosynthesis and applications. Chem. Soc. Rev. (2009). https://doi.org/10.1039/b816681c
27. S. Saha, P. Samanta, N. Chandra, T. Kuila, A review on the heterostructure nanomaterials for supercapacitor application. J.

Energy Storage **17**, 181–202 (2018). https://doi.org/10.1016/j.est.2018.03.006
28. N. Parveen, N. Mahato, M. Omaish, M. Hwan, Enhanced electrochemical behavior and hydrophobicity of crystalline polyaniline @ graphene nanocomposite synthesized at elevated temperature. Compos. B **87**, 281–290 (2016). https://doi.org/10.1016/j.compositesb.2015.10.029
29. S. Dhibar, P. Bhattacharya, G. Hatui, S. Sahoo, C.K. Das, transition metal-doped polyaniline/single-walled carbon nanotubes nanocomposites: efficient electrode material for high performance supercapacitors. ACS Sustain. Chem. Eng. (2014). https://doi.org/10.1021/sc5000072
30. T. Sen, S. Mishra, N.G. Shimpi, A β Cyclodextrin based binary dopant for polyaniline: structural, thermal, electrical, and sensing performance. Mater. Sci. Eng. B **220**, 13–21 (2017). https://doi.org/10.1016/j.mseb.2017.03.003
31. H. Gu, X. Xu, J. Cai, S. Wei, H. Wei, H. Liu, D.P. Young, Q. Shao, S. Wu, T. Ding, Z. Guo, Controllable organic magnetoresistance in polyaniline coated poly(p-phenylene-2,6-benzobisoxazole) short fibers. ChemComm (2019). https://doi.org/10.1039/c9cc04789a
32. Y. Ma, Z. Zhuang, M. Ma, Y. Yang, W. Li, M. Dong, S. Wu, T. Ding, Z. Guo, Solid polyaniline dendrites consisting of high aspect ratio branches self- assembled using sodium lauryl sulfonate as soft templates: synthesis and electrochemical performance. Polymer (Guildf) **182**, 121808 (2019). https://doi.org/10.1016/j.polymer.2019.121808
33. Q. Hu, N. Zhou, K. Gong, H. Liu, Q. Liu, Intracellular polymer substances induced conductive polyaniline for improved methane production from anaerobic wastewater treatment. ACS Sustain. Chem. Eng. (2019). https://doi.org/10.1021/acssuschemeng.8b05847
34. U. Bogdanovic, V. Vodnik, M. Mitric, S. Dimitrijevic, S.D. Skapin, V. Zunic, M. Budimir, M. Stoiljkovic, Nanomaterial with high antimicrobial efficacy copper/polyaniline nanocomposite. ACS Appl. Mater. Interfaces (2015). https://doi.org/10.1021/am507746m
35. D. Zhou, B. Che, X. Lu, Rapid one-pot electrodeposition of polyaniline/manganese dioxide hybrids: a facile approach to stable high-performance anodic electrochromic materials. J. Mater. Chem. C **5**, 1758–1766 (2017). https://doi.org/10.1039/C6TC05216A
36. L. Horta-romarís, M.V. González-rodríguez, A. Lasagabáster, Thermoelectric properties and intrinsic conduction processes in DBSA and NaSIPA doped polyanilines. Synth. Met. **243**, 44–50 (2018). https://doi.org/10.1016/j.synthmet.2018.06.002
37. S. Cho, K. Shin, J. Jang, Enhanced electrochemical performance of highly porous supercapacitor electrodes based on solution processed polyaniline thin films. ACS Appl. Mater. Interfaces **5**, 9186–9193 (2013)
38. A.K. Mukherjee, R. Menon, Role of mesoscopic morphology in charge transport of doped polyaniline. Pramana **58**, 233–239 (2002)
39. D. Ghosh, S. Giri, A. Mandal, C.K. Das, Supercapacitor based on H^+ and Ni^{2+} co-doped polyaniline–MWCNTs nanocomposite: synthesis and electrochemical characterization. RSC Adv. **3**, 11676 (2013). https://doi.org/10.1039/c3ra40955d
40. C. Anju, S. Palatty, Ternary doped plyaniline-metal nanocomposite as high performance supercapacitive material. Electrochim. Acta **299**, 626–635 (2019)
41. M. Vellakkat, A. Kamath, S. Raghu, S. Chapi, D. Hundekal, Dielectric constant and transport mechanism of percolated polyaniline nanoclay composites. Ind. Eng. Chem. Res. **53**, 16873–16882 (2014)
42. J. Jeon, J.O. Neal, L. Shao, J.L. Lutkenhaus, Charge storage in polymer acid-doped polyaniline-based layer-by- layer electrodes. ACS Appl. Mater. Interfaces. **5**, 10127–10136 (2013)
43. M.H. AbdelRehim, A.M. Youssef, H. Al-Said, T. Gamal, M. Aboaly, Polyaniline and modified titanate nanowires layerby-layer plastic electrode for flexible electronic device applications. RSC Adv. **6**, 94556 (2016)
44. X.S. Du, C.F. Zhou, Y.W. Mai, Facile synthesis of Hierarchical polyaniline nanostructures with dendritic nanofibers as scaffolds. J. Phys. Chem. C **112**, 19836–19840 (2008). https://doi.org/10.1021/jp8069404
45. S. Cho, M. Kim, J.S. Lee, J. Jang, Polypropylene/polyaniline nanofiber/reduced graphene oxide nanocomposite with enhanced electrical, dielectric, and ferroelectric properties for a high energy density capacitor. ACS Appl. Mater. Interfaces **7**, 22301–22314 (2015). https://doi.org/10.1021/acsami.5b05467
46. J. Zhu, H. Gu, Z. Luo, N. Haldolaarachige, D.P. Young, S. Wei, Z. Guo, Carbon nanostructure-derived polyaniline metacomposites: electrical, dielectric, and giant magnetoresistive properties. Langmuir **28**, 10246–10255 (2012). https://doi.org/10.1021/la302031f
47. K. Sun, J. Xin, Z. Wang, S. Feng, Z. Wang, R. Fan, H. Liu, Weakly negative permittivity and low frequency dispersive behavior in graphene/epoxy metacomposites. J. Mater. Sci.: Mater. Electron. (2019). https://doi.org/10.1007/s10854-019-01846-4
48. X. Yao, X. Kou, J. Qiu, M.G. Moloney, Generation mechanism of negative dielectric properties of metallic oxide crystals/PANI. Composites (2016). https://doi.org/10.1021/acs.jpcc.5b12352
49. K.L. Bhowmik, K. Deb, A. Bera, R.K. Nath, B. Saha, Charge transport through polyaniline incorporated electrically conducting functional paper charge transport through polyaniline incorporated electrically conducting functional paper. J. Phys. Chem. C (2016). https://doi.org/10.1021/acs.jpcc.5b08650
50. C. Dhand, M. Das, M. Datta, B.D. Malhotra, Biosensors and bioelectronics recent advances in polyaniline based biosensors. Biosens. Bioelectron. **26**, 2811–2821 (2011). https://doi.org/10.1016/j.bios.2010.10.017
51. C.M. De León-almazan, I.A. Estrada-moreno, U. Páramo-garcía, J.L. Rivera-armenta, Polyaniline/clay nanocomposites. a comparative approach on the doping acid and the clay spacing technique. Synth. Met. **236**, 61–67 (2018). https://doi.org/10.1016/j.synthmet.2018.01.006
52. M. Shi, Y. Zhang, M. Bai, B. Li, Facile fabrication of polyaniline with coral-like nanostructure as electrode material for supercapacitors. Synth. Met. **233**, 74–78 (2017). https://doi.org/10.1016/j.synthmet.2017.09.007
53. S.K. Simotwo, C. Delre, V. Kalra, Supercapacitor electrodes based on high-purity electrospun polyaniline and polyaniline-carbon nanotube nanofibers. ACS Appl. Mater. Interfaces. (2016). https://doi.org/10.1021/acsami.6b03463
54. D. Xu, Q. Xu, K. Wang, J. Chen, Z. Chen, Fabrication of Free-Standing Hierarchical Carbon Nano fi ber/Graphene Oxide/Polyaniline Films for Supercapacitors. ACS Appl. Mater. Interfaces. **6**, 200–209 (2014)
55. W. Fan, C. Zhang, W.W. Tjiu, K.P. Pramoda, C. He, T. Liu, Graphene-wrapped polyaniline hollow spheres as novel hybrid electrode materials for supercapacitor applications. ACS Appl. Mater. Interfaces (2013). https://doi.org/10.1021/am4003827
56. A.K. Thakur, A.B. Deshmukh, R. Bilash, I. Karbhal, M. Majumder, M.V. Shelke, Facile synthesis and electrochemical evaluation of PANI/CNT/MoS 2 ternary composite as an electrode material for high performance supercapacitor. Mater. Sci. Eng. B **223**, 24–34 (2017). https://doi.org/10.1016/j.mseb.2017.05.001

57. J. Plawan Kumar, K. Santosh Singh, G. Suresh, K. Sreekumar, B. Nirmalya, Pb2+—N bonding chemistry: recycling of polyaniline-pb nanocrystals waste for generating high-performance supercapacitor electrodes. J. Phys. Chem. C (2015). https://doi.org/10.1021/acs.jpcc.5b11217
58. A. Sajedi-moghaddam, C.C. Mayorga-martinez, D. Bous, Black phosphorus nano flakes/polyaniline hybrid material for high-performance pseudocapacitors (2017). https://doi.org/10.1021/acs.jpcc.7b06958
59. L. Mieko, D. Alves, D.L. Almeida, S.S. Oishi, A.B. Couto, Constituent material in fl uence on the electrochemical performance and supercapacitance of PANI/diamond/CF composite. Mater. Sci. Eng. B **228**, 249–260 (2018). https://doi.org/10.1016/j.mseb.2017.12.004